JOURNAL OF MATERIALS SCIENCE 29 (1994) 2860–2866

# The influence of elastic mismatch between indenter and substrate on Hertzian fracture

P. D. WARREN, D. A. HILLS*
*Departments of Materials* and * *Engineering Science, Oxford University, Parks Road, Oxford OX1 3PH, UK*

This paper is concerned with indentation testing of brittle materials. It is shown that a mismatch of elastic constants between the indenter and component being tested has a profound influence on the stress state induced. It is shown that the development of surface flaws into cracks is severely impeded if the indenter is more rigid than the substrate and vice versa. A quantitative assessment of this phenomenon, in terms of both the contact stress field generated and the stress intensity factor experienced by defects, is given. This permits a more precise determination of either the fracture toughness or the surface flaw distribution to be made.

## 1. Introduction

It is well known that pressing a spherical indenter normally into a perfectly brittle material will cause surface flaws to develop into a ring crack [1]. The ring often simultaneously extends and flares out into the frustum of a cone [2] if the surface is well polished, but this development may not happen unless the load is increased further. This phenomenon, first discovered about a hundred years ago [3], was for a long time regarded as little more than a curiosity. More recently, however, with the advent of the use of ceramic elements in an increasingly wide range of mechanical and electrical engineering applications, the potential of the test as a semi-destructive means of measuring fracture toughness or surface integrity has been realized. The test is potentially the brittle material equivalent of the hardness test conducted on a ductile material: it gives the opportunity to determine toughness whilst damaging only a small portion of the component. The principal difficulties in employing the test on a routine basis are twofold:

1. Because the crack generated is almost entirely subsurface, leaving only a ring visible on the surface, it is not possible to measure the size of the developed crack in an opaque material easily, or the load at which this occurs. To a large extent the problem of finding the latter parameter may be overcome by attaching an acoustic emission sensor to the substrate, which is readily capable of detecting the spontaneous growth of the crack, and although this does not provide such a complete set of information as knowing the final geometry it is, nevertheless, invaluable in determining with great precision the critical stress intensity factor for development of the ring crack.

2. In a normal Hertzian indentation the zone of tension is confined to a very small annular ring, and the spherical or hydrostatic component of stress is very much greater in magnitude within the zone immediately beneath the indenter. Indeed, the subsurface deviatoric stress, whilst smaller in magnitude than its spherical counterpart, nevertheless dominates the magnitude of the maximum tension by a significant amount. Therefore, in a great many cases, these attributes of the stress field mean that plasticity precedes brittle fracture, if the material has any ductility at all, and particularly if the surface finish is very good. It is very difficult, for example, to carry out an indentation test on PMMA which induces a ring crack without incurring gross plastic flow first in what is normally thought of as a brittle material [4]. It is usually found that the scale of the test also has an important influence on the effect of indentation: tests carried out using micro-indenters produce a well-defined crack system whilst geometrically similar tests carried out at the bulk scale may often lead to lateral fracture and disintegration of the specimen.

In this paper we will concentrate our attention on the second problem, and show that it is straightforward to enhance the growth of surface defects by using an indenter which is more compliant than the object being tested. This phenomenon received attention from Johnson *et al.* [5], who were the first to notice that an elastic mismatch between the contacting bodies will give rise to the presence of shearing tractions, and hence a modified contact stress field. To understand the origin of this effect, consider the case of an elastic sphere pressed on to an elastically dissimilar, frictionless half-plane to form a Hertzian contact of radius $a$ (Fig. 1). Particles lying on the surface of each sphere will move radially inwards in proportion to $(1 - 2\nu)/\mu$, where $\nu$ is Poisson's ratio and $\mu$ is the modulus of rigidity. As the two bodies are dissimilar there will be a relative displacement of any initially coincident pair of surface particles, and the one in the more compliant body, i.e. the one having a larger value of $(1 - 2\nu)/\mu$, will displace more. This relative motion will, however, be resisted by the presence of interfacial friction, which will therefore act radially


0022–2461 

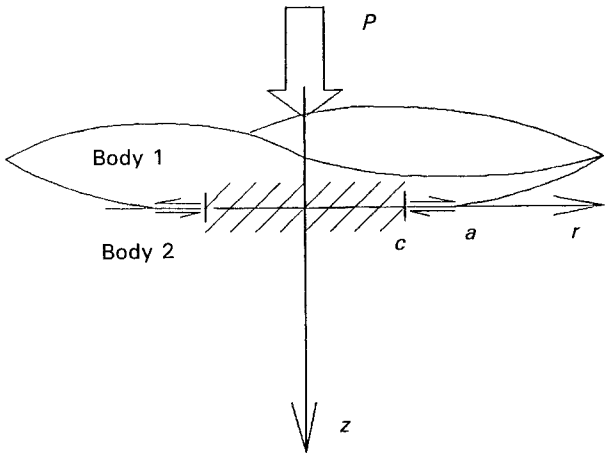


*Figure 1* Two dissimilar elastic spheres pressed together by a normal force, $P$; the radial surface displacements in bodies 1 and 2 differ if their elastic constants differ.

outwards on the more compliant body, and radially inwards on the less compliant one. Further, these shearing tractions will cause a change in the relative curvature of the contacting bodies, which will in turn influence the pressure distribution. It will therefore be seen that the contact problem itself is much more complex than that occurring between elastically similar bodies. In practice the magnitude of the influence of shearing tractions on the surface normal displacement is small, so that the contact pressure remains approximately Hertzian, and any differences will here be neglected [6].

The import of the above observations is that the ideal indenter is more compliant, harder, but tougher than the substrate being tested if the zone of tension is to be maximized, as will be shown.

## 2. Theory

### 2.1. Contact stress field

The state of stress induced by normal indentation by a sphere has been known for some time [7], and so attention is concentrated on the influence of the radial shearing tractions produced by mismatch. This problem was first addressed by Spence [8], who showed that the contact patch consists of a central stick zone where corresponding particles on the two bodies are adhered, surrounded by an annulus of slip in which the shear traction is limited by the coefficient of friction between the bodies, $f$. In axisymmetric problems involving elastic mismatch it may be shown that the influence of the mismatch may be quantified by a single dimensionless composite parameter due to Dundurs [9], namely

$$\beta = \frac{[(1-2\nu_1)/\mu_1] - [(1-2\nu_2)/\mu_2]}{2A} \quad (1)$$

where

$$A = \frac{1-\nu_1}{\mu_1} + \frac{1-\nu_2}{\mu_2}$$

is the composite compliance of the bodies and the subscripts 1, 2 refer to the two contacting bodies. The form of the contact shear traction distribution arising is complex, and the boundary between the stick and slip regions is located at a radius $ac$, where $c$ is given by

$$\frac{f}{\beta} = \frac{Q_0(c)}{cK(c')} \quad (2)$$

where

$$c'^2 = 1 - c^2$$

$$Q_0(x) = \frac{1}{2}\ln\left(\frac{1+x}{1-x}\right)$$

and $K(\ )$ is the complete elliptic integral of the first kind and $a$ is the radius of the contact disc. This equation is plotted in Fig. 2. If the coefficient of friction between the two bodies is very low the stick zone will shrink towards a point, and the slip annulus may be expected to extend over the entire contact disc. When this is so the shear traction distribution is straightforward, and is given by

$$\frac{q(r)}{fp_0} = (1-r^2)^{1/2}\,\mathrm{sgn}\,\beta \qquad 0 < r < 1 \quad (3)$$

where $q(r)$ is the shear traction, $p_0$ is the peak Hertzian contact pressure and the coordinate set has been normalized with respect to the radius of contact $a$. If, taking the other limit, Dundurs' constant is very low, stick will persist over almost the entire contact. This problem was investigated by Goodman [6], who showed that

$$\frac{q(r)}{\beta p_0} = \frac{r}{\pi}\int_0^{r'} \frac{\ln x\,\mathrm{d}x}{(1-x^2)^2} \qquad 0 < r < 1 \quad (4)$$

where $r'^2 = 1 - r^2$. In the general case neither of these idealizations is appropriate, and the solution is needed [8]. This is complex to evaluate, and in its original form described only what arises beneath a flat-ended punch, rather than a Hertzian indenter. From this the solution for a sphere may be found by transformation. For a flat-ended punch

$$q_B = \frac{fp_0}{2(1-r^2)^{1/2}}[1 - \Psi(r,c)]\,\mathrm{sgn}\,\beta \qquad 0 < r < 1 \quad (5)$$

where

$$\Psi(r,c) = 0 \qquad c \leqslant r \leqslant 1$$

$$= \frac{2}{\pi}\left[wr\int_0^{\pi/2} \frac{\mathrm{d}\theta}{[1-(1-r^2)\sin^2\theta](1-c'^2\sin^2\theta)^{1/2}} - \frac{CK(c')}{r}\left(\frac{w}{c} - \frac{Q_0(w)}{Q_0(c)}\right)\right] \qquad 0 \leqslant r \leqslant c \quad (6)$$

and

$$w^2 = \frac{c^2 - r^2}{l - r^2}$$

Equations 5 and 6 describe the shear traction distribution for a punch. The corresponding solution for a spherical indenter is given by

$$q(r) = 2r\int_r^1 \frac{q_B(t)\,\mathrm{d}t}{t^2} \quad (7)$$

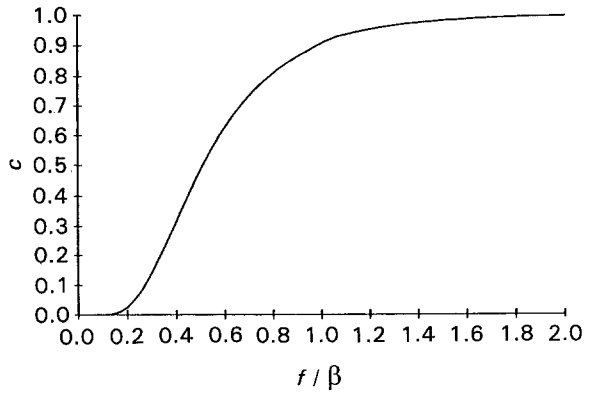


*Figure 2* The size of the stick zone radius $c$, normalized with respect to the radius of the contact disc $a$, as a function of the ratio $f/\beta$.

The complete state of stress at any point induced by the traction distributions corresponding to Equations 3–5 has been evaluated [10] and details will not be reproduced here. Inevitably, numerical methods are needed to evaluate the stress at subsurface points. However, the principal effect of the shear is on the surface state of stress; indeed the shear traction distribution is self-equilibrating, i.e. it has no resultant, and so its influence is short-lived. Nevertheless, this is precisely the region in which crack development takes place, and we will therefore consider it in some detail. For the surface, the stress components induced by radial shear ($\sigma_{rr}$ and $\sigma_{\theta\theta}$) may be written in the closed form given by Hills and Sackfield [10] and are, for the case of partial slip at the interface

$$\sigma_{rr} = \frac{2(1-\nu)}{r^2} I - \frac{2}{r}\left(\frac{dI}{dr}\right) \quad (8)$$

$$\sigma_{\theta\theta} = \frac{2(1-\nu)}{r^2} I - \frac{2\nu}{r}\left(\frac{dI}{dr}\right) \quad (9)$$

where, within the stick zone

$$\left.\begin{aligned} \frac{3\pi I}{2\beta p_0} &= \frac{1-p^3}{2} + Mr^2 \\ \frac{1}{\beta p_0}\left(\frac{dI}{dr}\right) &= pr + \frac{4}{\pi} Mr^2 \end{aligned}\right\} \quad 0 \leqslant r \leqslant c \quad (10)$$

and

$$M = \frac{1+c^2}{2c^2} Q_0(c) - \frac{1}{2c} - \frac{Ec' Q_0(c)}{c^2 K(c')}$$

whilst within the slip zone

$$\frac{3\pi I}{2p_0} = \beta\left[\lambda - p^2 \tan^{-1}\left(\frac{pc}{\nu}\right)\right] + 3f \int_c^r \frac{t^2}{(r^2-t^2)^{1/2}} \times [K(t') - E(t')]\,dt \qquad c \leqslant r \leqslant 1 \quad (11)$$

$$\frac{\pi}{2p_0}\left(\frac{dI}{dr}\right) = \beta\left[pr \tan^{-1}\left(\frac{pc}{\nu}\right) + r\nu Q_0(c) + 2r(r-\nu)M\right] + fr \times \int_c^r \frac{K(t') - 2E(t')\,dt}{(r^2-t^2)^{1/2}} \qquad c \leqslant r \leqslant 1$$

where

$$\lambda = \theta + M\left[2r^3 + \nu^3 - 3\nu r^2 - \frac{\nu}{2}(3 - c^2 - 2r^2) \times Q_0(c) - \frac{\nu c}{2}\right]$$

$$\nu^2 = r^2 - c^2$$

$$\sin\theta = c/r$$

Lastly, exterior to the contact

$$\frac{3\pi I}{2p_0} = \beta\left[\lambda - q^3 Q_0\left(\frac{cq}{\nu}\right)\right] + 3f \times \int_c^1 \frac{t^2}{(r^2-t^2)^{1/2}} [K(t') - E(T')]\,dt \qquad r \geqslant 1 \quad (12)$$

$$\frac{\pi}{2p_0}\left(\frac{dI}{dr}\right) = \beta\left[-\frac{c}{3r\nu} + M\left(2r^2 - \frac{r^3}{\nu} - \nu r\right)\right] - \frac{Q_0(c)}{6}\left[\frac{r}{\nu}(3 - c^2 - 2r^2) - 4r\nu\right] - \frac{rc}{6\nu} - qrQ_0\left(\frac{cq}{\nu}\right) - \frac{cq^2}{3r\nu} + fr\left(\frac{c}{\nu}[K(c') - E(c')] + \int_c^1 \frac{K(t') - 2E(t')\,dt}{(r^2-t^2)^{1/2}}\right) \qquad r \geqslant 1$$

where $K(\ )$, $E(\ )$ are complete elliptic integrals. Complex as these expressions are, they at least prove straightforward to evaluate. It should be emphasised that these equations relate only to the surface itself, and that stress gradients in the $z$ direction are extremely severe, so that for cracks of finite depth the complete interior stress field may be needed. Nevertheless, the above results are of some value, and it is quite impossible to express the interior stresses in closed form. Of principal interest in the present problem is the radial direct stress which lies in a principal direction at the surface, and hence propels the crack in its initial stages, and this is shown in Fig. 3. It is very clear from the figure that the shearing stresses have a profound influence on $\sigma_{rr}$, although it should be noted that the stress component associated with the shear is normalized with respect to the coefficient of friction. Qualitatively, two features are apparent; first, that the magnitude of the maximum tension may easily be doubled compared with the frictionless case, and secondly that the area over which an appreciable tension exists in the surface is greatly increased, and may now persist under the contact patch itself.

It should be recalled that the stresses calculated as due to the frictional shear have an equal magnitude in the two contacting bodies, but are of opposite sign; they are tensile in the less compliant body and compressive in the more compliant body. Historically this effect was first considered in relation to the indentation of glass by a steel ball, so that the shearing stress actually has the effect of inhibiting crack growth.

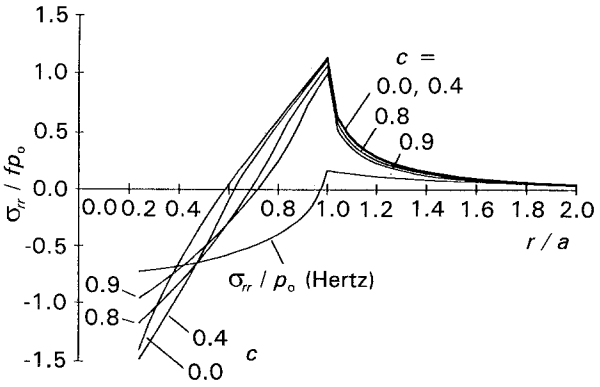


*Figure 3* Radial direct stress lying in the surface, $\sigma_{rr}$, as a function of radial position $r$, for partial slip, $\nu = 0.25$. $c$ is the normalized radius of the stick zone.

However, in relation to the indentation test of materials having some limited ductility it is seen that it would be desirable to use a more compliant indenter in order to encourage crack development, so that this precedes plastic flow.

The "bulk" contact field may be used to infer certain characteristics of the growth of Hertzian ring and cone cracks. First, if it is assumed that the crack is propelled by the more positive principal stress, it is clear that development can occur only in regions of net tension, and this zone is shown in Fig. 4. This shows that the cone crack is restricted to a shallow frustum in the case of like materials, but is somewhat extended if a compliant indenter is used. Secondly, some indication of the likely form of the crack may be gained from a plot of stress trajectories (Fig. 5). These are lines whose tangent at any point lies in the direction of the more positive principal stress, and are consistent with the form of the frustum of a cone usually observed. The presence of the crack will, of course, change the stress field experienced considerably, but Figs 4 and 5 nevertheless provide an encouraging qualitative explanation of the crack shape.

## 2.2. Crack tip stress intensities

Cracks propelled by contact stress fields invariably exist in extremely steep stress gradients, and the utmost care is therefore needed in the evaluation of the stress intensity factors. Further, in the present problem, when once the fully developed cone crack has developed it is impossible to ignore the axisymmetric nature of the geometry, and this makes the analysis even more challenging, although at least one solution to the full Hertzian cone crack has been published [11].

In a real indentation test, pre-existing surface defects may well be in the form of semi-circular (thumbnail) cracks. As the contact load is increased the stress intensity factor around the crack front increases until the fracture toughness value is reached, at which point the crack "runs round" to form a ring, and, as stated at the outset, may simultaneoulsy flare into the frustum of a cone. The solution we will present here applies to plane cracks, i.e. those existing in a two-dimensional stress field. We may therefore view the solution on two

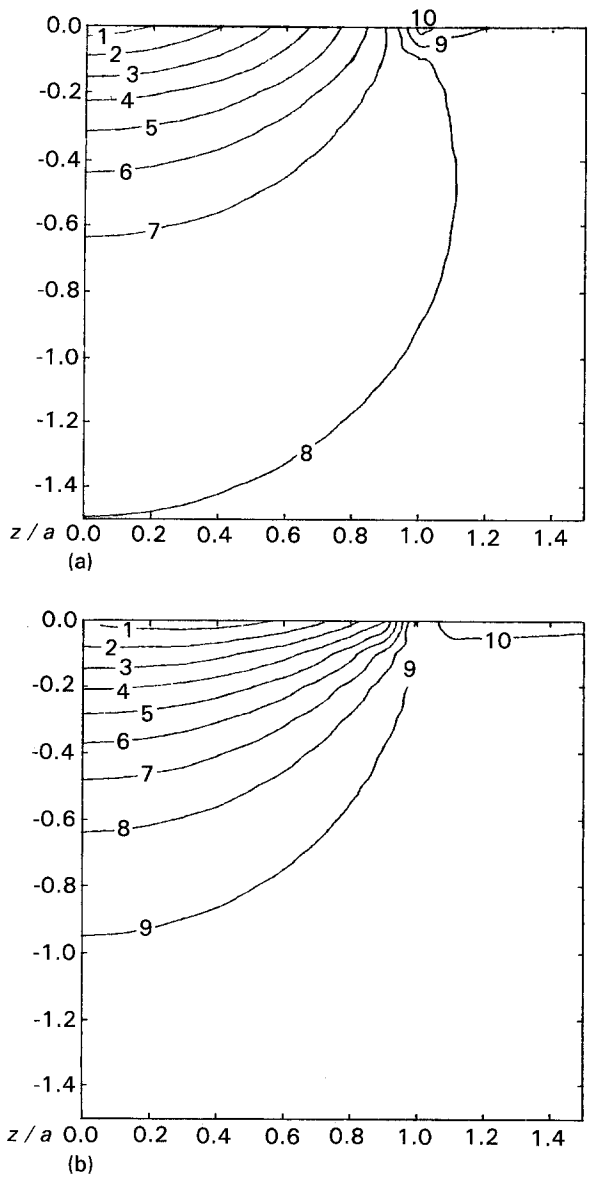


*Figure 4* More positive principal stress contours beneath a normally loaded dissimilar elastic contact, $\beta = 0.204$. (a) Less compliant body: values of contours $\sigma_{max}/P_0$ are (1) $-0.933$, (2) $-0.800$, (3) $-0.667$, (4) $-0.533$, (5) $-0.400$, (6) $-0.267$, (7) $-0.134$, (8) $-0.267 \times 10^{-3}$, (9) 0.133, (10) 0.266. (b) More compliant body: values of contours $\sigma_{max}/P_0$ are (1) $-0.488$, (2) $-0.430$, (3) $-0.371$, (4) $-0.313$, (5) $-0.254$, (6) $-0.196$, (7) $-0.137$, (8) $-0.786 \times 10^{-1}$, (9) $-0.201 \times 10^{-1}$, (10) $0.384 \times 10^{-1}$.

different scales:

1. It may be viewed as an approximate solution to the stress intensity factor obtaining at the bottom of the semi-circular flaw, and therefore the value which controls the onset of development into a crack of macroscopic dimensions.

2. When a self-arrested crack in the form of a simple ring develops, it may be viewed as the stress intensity factor existing around the bottom of the ring crack: thus, crack growth will arrest when the stress intensity factor at this point falls below the fracture toughness value. It should be emphasized that this self-arrest may not always be experienced in practice, and that the solution will only be valid if the crack depth is much less than the radius of the contact disc, i.e. $s \gg d$ (Fig. 6).

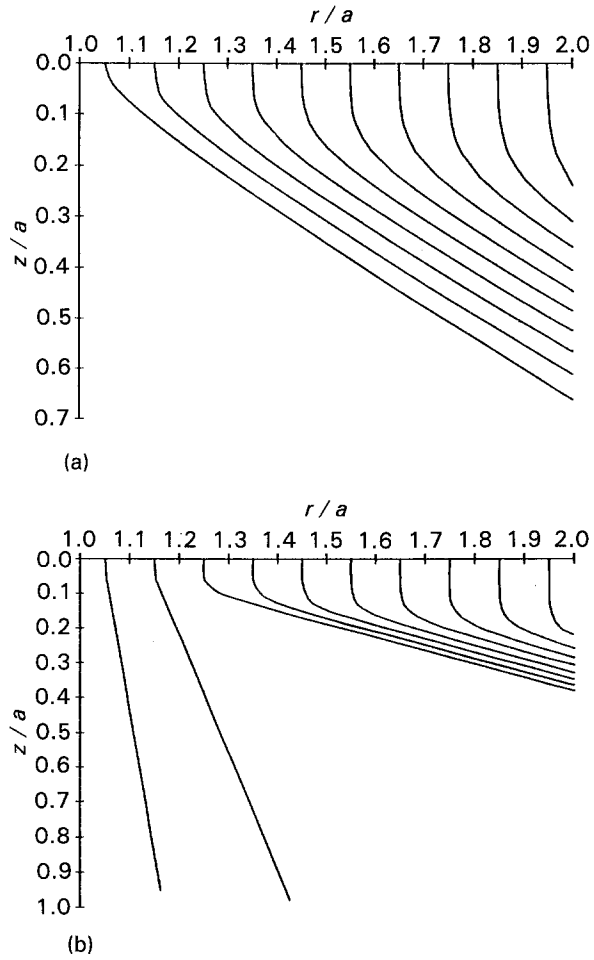


*Figure 5* Trajectories of the principal stress direction beneath a normally loaded dissimilar elastic contact, $\beta = 0.204$, (a) in less compliant body and (b) in more compliant body.

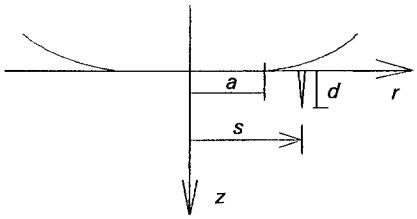


*Figure 6* Geometry of crack in the neighbourhood of the contact.

A suitable method to determine the stress intensity factor for this problem is to distribute infinitesimal displacement discontinuities (or dislocations) along the length of the crack, in order to render the crack faces traction-free. This technique has been used extensively before, and an introductory paper [12] should be consulted for details. Here we will restrict ourselves to writing down the integral equation which describes the traction-free state of the crack, namely

$$O = \tilde{\sigma}_{ri}(\xi) + \frac{\mu}{\pi(\kappa + 1)} \int_0^d B_i(\xi) K(\xi, z) \mathrm{d}z \; i = r, z \tag{13}$$

where $\tilde{\sigma}_{ri}$ is the traction along the line of the crack in its absence, $\kappa$ is Kolosov's constant, $B_i$ is the unknown dislocation density and the function $K(\xi, z)$ gives the value of the stress at point $\xi$ due to a dislocation of unit strength at point $z$. This function and a description of the solution technique used is given elsewhere [12] and will not be repeated here. However, it should be stated that the procedure described is preferred because it can handle the stress gradient extremely well, and gives rise to a set of simultaneous linear algebraic equations representing the integral Equation 13 whose solution may easily be found, and which provides an efficient means of determining the stress intensity factor.

## 3. Results

In this section we display the stress intensity factors found for short cracks growing normally inwards from the free surface. It is impossible to present a comprehensive set of results to the problem posed as there are so many independent variables, namely Dundurs' constant $\beta$, the coefficient of friction $f$, the dimensionless depth of the crack $(d/a)$ and the dimensionless radius of the crack's location $(s/a)$ (Fig. 6). It will be recalled, however, that with the approximations made in determining the shear traction distribution described in Section 2.1 it is possible to remove one of the independent quantities describing the surface traction distribution. Fig. 7a and b show the crack tip stress intensities in modes I and II, respectively, for a contact where slip persists everywhere: this may be expected to be a good idealization when $f/\beta \ll 1$, i.e. the elastic mismatch is great and the interface is moderately well lubricated. The values shown are for a crack located at $s/a = 1.2$, i.e. outside the contact disc, and positioned approximately at the point of maximum radial tension. The curves corresponding to $f = 0$ are those which would obtain in a contact between elastically similar components, whilst those where $f > 0$ relate to cracks located in the stiffer of the contacting bodies, i.e. the shear tractions are acting radially inwards on the body containing the crack.

We have used the device of quoting a negative value of $f$ for problems in which the shear tractions act radially outwards. This is no more than a convention, and the coefficient of friction is, of course, always positive; the curves shown for $f < 0$ therefore relate to cracks in the more compliant body. It will be recognized that in the latter case the tendency towards crack opening is greatly suppressed, and indeed for coefficients of friction greater in absolute magnitude than about 0.3 there may be little or no mode I loading of the crack tip at all. The mode II component of loading always vanishes when the crack is very short as the surface is devoid of shear tractions. However, in this region the shear stress distribution exhibits extremely steep gradients in the $z$ direction, and hence it is possible to obtain shear loading of either sign, depending on the depth of the crack (Fig. 7b). The absolute value of the mode II loading component is nevertheless very small in every case, and crack propulsion is dominated by mode I loading. In Fig. 7c and d analogous results are shown for contact–crack combinations where stick is assumed to persist everywhere. These solutions may be expected to be representative of real behaviour when $f/\beta \gg 1$, i.e. when the

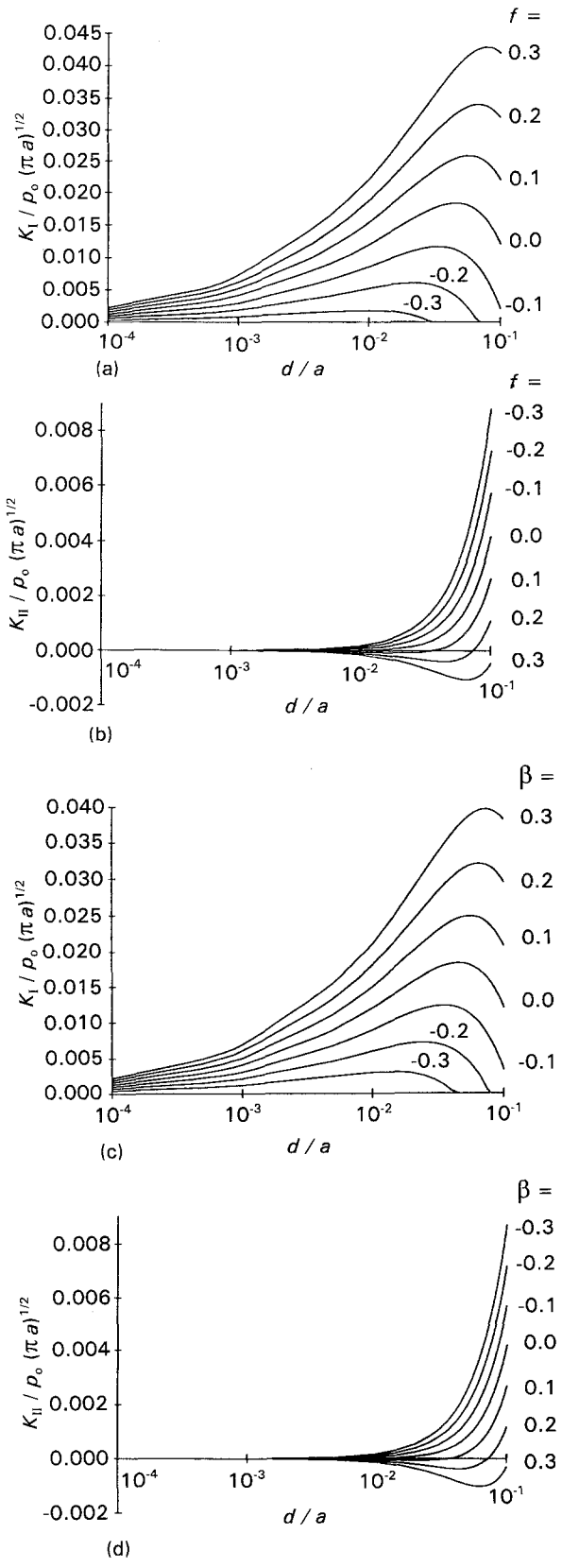


*Figure 7* Variation in stress intensity factors for a crack normal to the free surface, located at $s/a = 1.2$ and with $\nu = 0.25$: (a) and (b) relate to wholly slipping contacts and give values for modes I and II, respectively, whilst (c) and (d) relate to adhered contacts and again relate to modes I and II loading, respectively.

degree of material mismatch is modest and the interfacial coefficient of friction is large. The convention regarding the sign of $\beta$ used is consistent with that used for the coefficient of friction, i.e. if $\beta > 0$ the

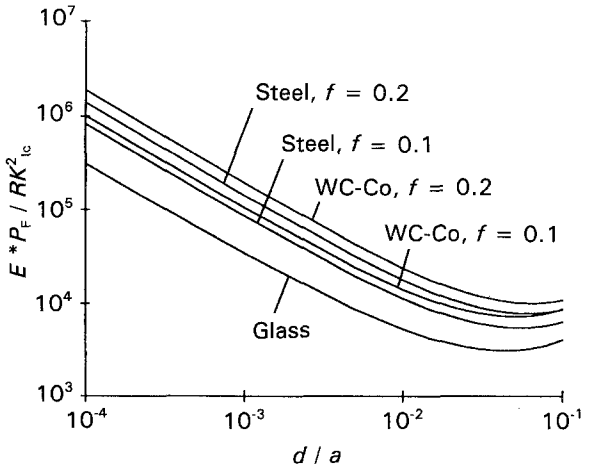


*Figure 8* Maximum mode I stress intensity factor experienced by a normal crack in a glass component when loaded by a steel or tungsten carbide indenter. The depth of the crack is $d/a$, and $s/a$ has been permitted to vary so that the location giving the maximum value of $K_I$ is utilized. $E^*$ is the reduced modulus of sphere and substrate, $K_{IC}$ is the fracture toughness, $R$ is the sphere radius and $P_F$ is the fracture load.

results apply to the stiffer material, whilst if $\beta < 0$ the results pertain to the more compliant material.

Fig. 8 shows results obtained with specific material combinations, and retaining the assumption of partial slip. Values given are for minimum fracture load, which is equivalent to the reciprocal of the maximum stress intensity factor in mode I, for the indentation of glass. The ordinate axis is normalized with respect to the load, material stiffness and contact geometry, and may be used to determine the contact force needed to achieve a particular stress intensity factor. The Poisson's ratio of glass is taken as 0.25, and the location of the crack has been permitted to take a range of values within which the stress intensity factor has been maximized. Results are shown for two kinds of indenter, namely steel and tungsten carbide, and two representative values of the coefficient of friction. It will be seen that the choice of indenter material has a profound influence on the crack driving force, regardless of the crack depth.

## 4. Summary

A comprehensive study of the influence of indenter elasticity on the crack driving force for Hertzian ring-type cracks has been conducted. The problem has been split into two parts, namely the determination of the contact stress field for frictional contact between elastically dissimilar materials, and the determination of crack tip stress intensities for plane cracks propelled by such a stress field. The results displayed show how the crack tip stress intensity factors experienced by such contacts may be widely influenced by the perturbation on a standard Hertzian contact stress field by frictional radial shearing tractions generated by the effects of elastic mismatch. It is particularly important to note the qualitative result that using an indenter which is more rigid than the component being tested causes a suppression of mode I crack loading, so that the influence of mode II loading becomes correspondingly more important, particularly for deeper initial

flaws, and that there is in any case a greater tendency towards crushing of the surface rather than the clean propulsion of a well-defined single crack.

It is valuable to know just how dissimilar the substrate and indenter may be before it is permissible to ignore the influence of elastic mismatch. To this end, the difference in the surface stresses (and hence the difference in the fracture loads for materials having the same toughness, providing the critical cracks are short) was calculated, including and excluding the influence of surface shearing tractions. This was done for two representative substrate materials under conditions of full stick. It was shown that for the absolute maximum $K_I$ values to be within 10% of the true value, the influence of mismatch could only be neglected if the absolute value of $\beta$ was less than 0.019 if $\nu = 0.14$, or 0.009 if $\nu = 0.34$. It is therefore apparent that in order to obtain accurate results either a virtually elastically identical identer must be employed, or due allowance for the presence of the radial shearing tractions must be made.

Copies of the FORTRAN code for use on a PC may be obtained from the authors to permit a wider range of variables to be covered.

## References


1. F. C. ROESLER, *Proc. Phys. Soc.* **69** (1956) 981.
2. B. R. LAWN and T. R. WILSHAW, *J. Mater. Sci.* **10** (1975) 1049.
3. F. AUERBACH, *Ann. Physik U. Chem.* **43**(5) (1891) 61.
4. D. A. HILLS, *Wear* **85** (1983) 107.
5. K. L. JOHNSON, J. J. O'CONNOR and A. C. WOODWARD, *Proc. Roy. Soc.* **A334** (1973) 95.
6. L. E. GOODMAN, *J. Appl. Mech.* **29** (1962) 515.
7. M. T. HÜBER, *Ann. Physik* **14** (1904) 153.
8. D. A. SPENCE, *J. Elasticity* **5** (1975) 297.
9. J. DUNDURS, *J. Appl. Mech.* **36** (1969) 650.
10. D. A. HILLS and A. SACKFIELD, *ibid.* **109** (1987) 8.
11. Y. LI and D. A. HILLS, *ibid.* **58** (1991) 120.
12. D. NOWELL and D. A. HILLS, *J. Strain Anal.* **22**(3) (1987) 177.



*Received 14 September*
*and accepted 8 October 1993*